

## Histological and Immunohistochemical Study on the Protective Role of Coenzyme Q10 on Carbon Tetra Chloride -Induced Toxicity on the Renal Cortex of Adult Male Albino Rats

Asmaa Ibrahim Ahmed and Hagar Yousry Rady

Department of Anatomy and Embryology, Faculty of Medicine, Ain Shams University, Egypt

### ABSTRACT

**Introduction:** Carbon Tetra Chloride (CCl<sub>4</sub>) is a chemical toxin that induces oxidative stress. Coenzyme Q10 (CoQ10) is a naturally occurring antioxidant present in meat, fish, nuts.

**Aim of the Work:** Was to assess the protective effect of CoQ10 on Kidney injury following the exposure to Carbon Tetra Chloride (CCl<sub>4</sub>).

**Materials and Methods:** Forty-four adult male albino rats divided into three groups. Group I (control) included 24 rats, Group II (CCl<sub>4</sub>-treated group): included 10 rats that were injected intraperitoneally with CCl<sub>4</sub> solution at a dose of 0.1 ml / 100 gm B.W. twice weekly for 2 weeks. Group III (CCl<sub>4</sub>+ CoQ10-treated group): included 10 rats that were received concomitant intraperitoneal injections of CCl<sub>4</sub> at the same doses and the same duration as in group II, in addition to CoQ10 at a dose of 10 mg/kg B.W./day. At the end of experiment, all the rats were sacrificed; the kidneys were dissected and processed for microscopic examination (LM&EM). Immunostaining for iNos was done. The results were statistically analyzed.

**Results:** CCl<sub>4</sub> induce marked distortion of the renal cortical architecture. LM examination showed hypercellularity of glomerular tuft with obliteration of capsular space. Adhesion of the glomerular tuft to parietal layer of Bowman's capsule occurred. Also effacement of the foot process of podocyte was detected by EM. Renal cortical tubules revealed degenerative and necrotic changes. Interstitial tissue showed mononuclear inflammatory cell infiltrate and consequently fibrosis. This was confirmed by significant increase in area% of collagen fibers. iNos immunostaining showed significant increase in CCl<sub>4</sub> treated group compared to the control and treated groups. Serum BUN & creatinine revealed statistically significant increase in group II compared to group I & III. All these changes were ameliorated by administration of CoQ10 (group III).

**Conclusions:** CoQ10 can protect against CCl<sub>4</sub>-induced kidney injury.

**Received:** 22 July 2022, **Accepted:** 28 August 2022

**Key Words:** Carbon tetra chloride, coenzyme Q10, electron microscope, iNOS, kidney.

**Corresponding Author:** Asmaa Ibrahim Ahmed Othman, MD, Department of Anatomy and Embryology, Faculty of Medicine, Ain Shams University, Egypt, **Tel.:** +20 10 0766 7294, **E-mail:** asmaaibrahim96@yahoo.com

**ISSN:** 1110-0559, Vol. 46, No. 4

### INTRODUCTION

Xenobiotic & heavy metals induce nephrotoxicity<sup>[1]</sup>. The strongest poisonous and environmental pollutants xenobiotic is carbon tetrachloride (CCl<sub>4</sub>). It is frequently utilized in cleaning products, refrigerants, and fire extinguishers<sup>[2]</sup>. Humans are exposed to CCl<sub>4</sub> through their mouths, their lungs, and their skin<sup>[3]</sup>. Additionally, CCl<sub>4</sub> is frequently utilized in scientific research to create the best models that simulate oxidative damage in many circumstances in various organs<sup>[2,4]</sup>. Antioxidant chemicals might therefore be used to lessen the oxidative stress induced by this xenobiotic<sup>[5]</sup>. Plants, animals, and human tissues all contain a lipid-soluble molecule known as coenzyme Q10 (CoQ10), a benzoquinone complex<sup>[6]</sup>. Low-density lipoproteins carry it into the bloodstream after it is mostly biosynthesized in the Golgi apparatus and mitochondria from mevalonate, tyrosine, and vitamins C, B2, B9, and B12<sup>[7]</sup>. Some of the best food sources of CoQ10 include meat, fish, nuts. It is utilized in numerous conditions as a dietary supplement and as a co-therapy

with medication<sup>[8]</sup>. Due to its antioxidant properties, anti-inflammatory, immunomodulatory and anti-aging. CoQ10 has gained popularity in recent years<sup>[9,10,11]</sup>. The purpose of this study was to determine if CoQ10 might protect adult male albino rats' kidneys from the nephrotoxic effects of CCl<sub>4</sub> by histopathological, immunohistochemical, and biochemical studies.

### MATERIAL AND METHODS

#### Animals

Forty-four adult male albino rats Sprague Dawley strain (4-6 months old), weighing between 180 and 200 gm were procured. At the Medical Research Center, Faculty of Medicine, Ain Shams University Each two rats were kept in a medium-sized stainless-steel cage at a time, and the rats were given a week for accommodation. The rats were given a daily feed and free access to water (ad libitum) with good ventilation. They were also subjected to a 12-hour light/dark cycle.

## Drugs

### Induction of CCl<sub>4</sub>-induced nephrotoxicity

- Carbon tetrachloride (CCl<sub>4</sub>) were procured from Sigma-Aldrich Chemical Company (St. Louis, Missouri, USA).
- Extra-virgin olive oil obtained from (Saporito Foods Inc., Markham, Ontario, Canada).
- Preparation of CCl<sub>4</sub> solution:

CCl<sub>4</sub> was shortly made at the time of use and diluted in an equivalent volume of extra-virgin olive oil (ratio 1:1). It was administered intraperitoneally (IP) to rats twice a week at a dose of (0.1 ml / 100 g B.W.<sup>[12]</sup>).

### Preparation of (CoQ10) solution

- CoQ10 was procured from Arab Company for Pharmaceuticals
- Corn oil procured from EL- Gomhorea company.

CoQ10 was purchased as capsules, each capsule containing 30 mg of CoQ10 powder. The powder was dissolved in its vehicle in an equal volume of corn oil (ratio 1:1) and was then injected intraperitoneally to rats at a dose of 10 mg/kg B.W. /day<sup>[13]</sup>. So CoQ10 administered to the rats in the powder form dissolved in corn oil and then injected intraperitoneally

## Experimental Design

The rats were divided into three groups as follows

**Group I** (control group): contained 24 rats, that are further subdivided into:

- Subgroup IA (Negative control): contained 6 rats that were not given any treatment.
- Subgroup IB (Solvent control): contained 6 rats that received intraperitoneal injection of extra virgin oil (vehicle for CCl<sub>4</sub>) at a dose of 0.1 ml / 100 gm B.W. twice weekly<sup>[12]</sup>.
- Subgroup IC (Solvent control): contained 6 rats that received daily intraperitoneal injection of corn oil (vehicle for CoQ10) for 2 weeks.
- Subgroup ID: (CoQ10-control): contained 6 rats that were injected intraperitoneally with CoQ10 solution at a dose of 10 mg/kg B.W./day for 2 weeks<sup>[13]</sup>.

**Group II** (CCl<sub>4</sub>-treated group): contained 10 rats that were injected intraperitoneally with CCl<sub>4</sub> solution at a dose of 0.1 ml / 100 gm B.W. twice weekly for 2 weeks<sup>[12]</sup>.

**Group III** (CCl<sub>4</sub>+ CoQ10-treated group): contained 10 rats that received a simultaneous co administration of intraperitoneal injections with both solutions (CCl<sub>4</sub> and CoQ10) at the same doses and duration as in groups II and ID.

## Ethical Consideration

All animal procedures were done according to the recommendations of the "CARE" guidelines which conforms to the Guide for the Care and Use of Laboratory Animals published by the US National Institute of Health. (Eighth edition, 2011, published by The National Academies Press). The present study was conducted in accordance with the European Communities Council Directive of 24 November 1986 (86/609/EEC) and was applied as stated by the ethics committee of faculty of medicine, Ain Shams University (FMASU REC). All efforts were made to minimize animal suffering as well as to reduce the number of animals used.

### Sample collection

Using ether inhalation, all rats were anaesthetized at the end of the experiment (after 2 weeks). Blood venous samples of each rat were collected from the tail vein. Plasma was separated and used for biochemical assays. The anterior abdominal walls of the animals were incised; the kidneys were carefully dissected, obtained, and cut longitudinally to be exposed to various techniques. Specimens from left kidney were processed for paraffin, semi thin and ultrathin sections to be examined by the light and electron microscopes.

### light microscopic studies

Samples of the Rats' kidneys were collected included those with longitudinal cuts. The specimens were embedded in blocks of paraffin after they were fixed in 10% neutral-buffered formalin and dehydrated. Serial paraffin slices (5 µm thick) were made and then stained with Periodic Acid-Schiff (PAS) for glycogen identification, Masson's trichrome (MTC) stain to detect the distribution of collagen fibers and renal fibrosis, and Hematoxylin & Eosin (H&E)<sup>[14]</sup>. At the Anatomy Department, Faculty of Medicine, Ain Shams University, all sections were examined and photographed using an Olympus BX 40 light microscope (Olympus, Hamburg, Germany) linked to a Canon Inc. power shot A640 digital camera (Tokyo, Japan)

### Immunohistochemical study

#### Inducible nitric oxide synthase (iNOS)

Nitrous oxide (NO), a free radical, is produced by a family of enzymes called nitric oxide synthases (NOSs) by the oxidation of L-arginine (L-Arg). The iNOS, is inflammatory mediator. Overexpressed or dysregulated iNOS has been implicated in numerous pathologies. The CCl<sub>4</sub> administration in group II increased iNOS concentrations and show strong positive diffuse iNOS immunoreaction, and COQ10 administration in group III decreased iNOS concentrations. The iNOS reactivity was considered as brown cytoplasmic staining. The interpretation of the results considered both the staining intensity and the percentage of positive cells<sup>[45]</sup>

An avidin-biotin-peroxidase complex immunohistochemical method (Elite-ABC; Vector Laboratories, California, USA) against iNOS (1:200 dilutions; BD Bioscience, San Diego, California, USA) was used to examine the distributions of iNOS receptor subunits in the renal cortex in deparaffinized sections (5 mm)<sup>[15]</sup>

At the Anatomy Department, Faculty of Medicine, Ain Shams University, all sections were viewed and photographed using an Olympus BX 40 light microscope (Olympus, Hamburg, Germany) linked to a Canon Inc. power shot A640 digital camera (Tokyo, Japan).

### **Electron microscopic studies**

The samples were promptly cut into 1mm-diameter cubes, and they were then left to fix overnight at 4°C in 2.5 percent phosphate-buffered glutaraldehyde (pH 7.3). The specimens were next dehydrated in increasing grades of ethyl alcohol after they were postfixed for 1-2 hours in 1 percent buffered osmium tetroxide, cleaned in propylene oxide, and finally embedded in brand-new Epon blocks. Glass knives were used to cut semi-thin slices with a thickness of 1 µm on the LKB ultramicrotome, and they were dyed with 1 percent toluidine blue at pH 7.3. The chosen areas were then chosen after sections were examined under a light microscope by Olympus. On a Reichert ultra-microtome, 70-90 nm ultrathin slices were cut from specific blocks, mounted on copper grids, and stained with uranyl acetate and lead citrate<sup>[16]</sup>. These sections were examined using the Transmission Electron Microscope in Electron Microscope Unit, Faculty of Science, Ain Shams University.

### **Histomorphometric study and image analysis**

1. Area percentage of green color (represent collagen fibers deposition) were estimated using Masson's trichrome stained sections.
2. Area percentage of brown color (represent cytoplasmic iNOS immunoreactions) were estimated. The procedure was performed using deparaffinized immunohistochemically stained slides with avidin-biotin-peroxidase.

The data were collected using a Leica Qwin 500 Image Analyzer Computer System (Cambridge, England, UK) at Faculty of Medicine, Cairo University. Measurements were done at ×400 magnification. Measurements were registered from six microscopic fields per slide, six slides per rat, and six rats per group for each of the aforementioned parameters.

### **Statistical analysis**

The image analysis data was statistically analyzed using SPSS software (Statistical Package for Social Studies- version 13.0). The means of the various groups were compared using one-way analysis of variance (ANOVA). The Bonferroni Post Hoc test was employed to determine whether there was a difference between each

pair of groups. The probability determined the relevance of the data was by (*P. value*).  $P > 0.05$  was regarded as being non-significant.  $P \leq 0.001$  was regarded as highly significant,  $P \leq 0.05$  as significant<sup>[17]</sup>. Using MS Excel 2013, data were represented in tables and histograms.

### **Biochemical analysis**

The withdrawn venous blood from each rat was centrifuged with 5000 r/min for 10 min by using centrifuge and plasma was collected. Renal function was assessed by measurement of the level of Serum Creatinine and Blood Urea Nitrogen (BUN). Creatinine was estimated (the Rate-Blanked /Jaffe method) and BUN was measured (kinetic UV assay) using a Roche/Hitachi auto-analyzer. These biochemical studies were done in Ain-Shams Specialized Hospital labs

## **RESULTS**

### **Histological results**

Examination of sections of group I (four control subgroups) revealed almost similar structure of the renal cortex. Therefore, the following figures will be representative for all.

#### **Results of H&E stained sections**

**Group I (control group):** The H&E -stained sections demonstrated the normal structure of the renal cortex which formed of renal corpuscles, and proximal (PCT) as well as distal convoluted tubules (DCT). The interstitial tissue with numerous capillaries was present between the tubules and the glomeruli (Figure 1A). Each renal corpuscle consisted of glomerulus and Bowman's capsule. Bowman's capsule formed of outer partial layer and inner visceral layer. The partial layer consisted of simple squamous epithelium resting on basement membrane. The visceral layer consisted of podocytes. The Bowman's capsule included space called Bowman's space between visceral and parietal layer of Bowman's capsule (Figure 1B). PCT with narrow lumina were lined by tall columnar epithelium having basally situated rounded nuclei and, acidophilic cytoplasm. DCT were lined by simple low cuboidal epithelium with apically situated nuclei. They appeared to have a relatively wider lumina than the proximal convoluted ones. Nuclei of the interstitial cells of renal cortex were seen (Figure 1C).

**Group II (CCL4-treated group):** The H&E- stained sections demonstrated marked distortion of normal renal cortical architecture. Wide interstitial spaces were detected containing congested and dilated thick-walled blood vessels, together with perivascular and peritubular mononuclear inflammatory cell infiltrate. Cellular and hyaline casts were detected in the lumen of the tubules (Figure 2A). Some tubules showed eroded surface and others tubules with small dark stained nuclei were also seen (Figure 2B). Some glomeruli revealed hypercellularity, congested glomerular capillaries with obliterated Bowman's space. There were adhesions between Bowman's capsule and glomerular tuft of capillaries. Multiple pale stained cells originated from

parietal layer of Bowman's capsule and started to invade the glomerular capillary tuft were detected (Figure 2C). The convoluted tubules showed marked distortion with degeneration of their epithelial. The interstitium showed inflammatory cellular infiltrate and interstitial hemorrhage (Figure 2D). Cytoplasmic vacuolations of tubular cells were seen. Some tubules revealed denuded and exfoliated cells into the tubular lumina with the congested peritubular capillaries. The interstitium showed many spindle-shaped nuclei of fibroblast (Figure 2E). Some tubules showed intraluminal hyaline casts (Figure 2F).

**Group III** (CCl4 + CoQ10 treated group): The H&E-stained sections were similar to the control revealed apparent improvement of the structure of the renal cortex. Some tubules appear normal, but other tubules still show degenerative changes. The glomeruli appeared normal with patent capillary and normal Bowman's space (Figures 3 A,B).

#### Results of Toluidine blue stained semi thin sections

**Group I** (control group): In semi thin sections the podocytes with their distinguished nuclei were seen covering the capillaries, while the endothelial cells were lining the capillaries, and mesangial cells were seen between the glomerular tuft. The parietal layer of Bowman's capsule was also seen as single layer of flattened epithelial cells enclosing the glomerulus with Bowman's space in between (Figure 4A). The PCT were lined with tall dark stained columnar cells with basally situated rounded vesicular nuclei and showed apical brush border. The DCT were lined by low cuboidal cells with apically situated nuclei and pale stained cytoplasm (Figure 4B).

**Group II** (CCl4-treated group): In the semi thin sections hypercellularity of the glomeruli were seen (apparent increase of the nuclei of mesangial, endothelial cells and proliferating cells of partial layer of Bowman's capsule), the glomeruli with occluded lumina of their capillaries were also seen. Some tubules showed denuded surface and exfoliated nuclei (Figure 4C). Multiple tubular casts and degenerated cellular debris in the lumina of the tubules were seen (Figure 4D)

**Group III** (CCl4 + Co Q10 treated group): Semi thin sections were similar to control where they showed restoration of normal of the architecture of the renal corpuscle and tubules. The glomerular capillaries were patent. The PCT were lined by columnar cells with brush border and basally situated vesicular nuclei. DCT appeared normal. Few tubular cells showed vacuolated cytoplasm. The interstitial congested blood vessels were seen (Figure 4E).

#### Results of Masson's trichrome-stained sections

**Group I** (control group): The renal cortex showed few thin peri glomerular and peri tubular collagen fibers deposition (Figure 5A). **Group II** (CCl4-treated group): revealed apparent increase in the collagen fibers deposition around glomerular capillary tuft and around degenerated

tubules in the renal cortex (Figure 5B). **Group III** (CCl4 + CoQ10 treated group): showed restoration of normal appearance similar to the control with few peri glomerular and per tubular collagen fibers deposition (Figure 5C).

#### Results of Periodic Acid-Schiff (PAS) stained sections

**Group I** (control group): Corpuscle showed presence of PAS (+) basement membrane of both glomerular capillaries and parietal layer of the Bowman's capsule and PAS (+) mesangial matrix. All tubules showed PAS (+) BM. PCT showed PAS (+) apical brush borders (Figure 6A). **Group II** (CCl4-treated group): Apparent increase in the PAS (+) reaction in the mesangial matrix and BM of the parietal layer of the Bowman's capsule was detected. All tubules showed apparent increase in the PAS (+) BM. Some tubules showed PAS (+) hyaline casts. PCT showed apparent decrease in PAS (+) reaction of brush border (Figure 6B). **Group III** (CCl4 + CoQ10 treated group): Displayed normal PAS (+) reaction in the renal corpuscle and tubules similar to the control (Figure 6C).

#### Immunohistochemical Results of iNOS

**Group I** (control group): Renal cortex showed negative cytoplasmic reactivity for iNOS in glomeruli. Weak cytoplasmic reactivity was detected in the proximal tubular cells (Figure 7A). **Group II** (CCl4-treated group): Some tubular cells showed weak iNOS, other tubules showed strong iNOS (Figure 7B). **Group III** (CCl4 + CoQ10 treated group): Most of the tubules showed weak iNOS reactivity (Figure 7C).

#### Transmission Electron Microscopic Results (TEM)

Ultrastructural examination of all sections of the rat's renal cortex of **group I** showed: renal corpuscle contained Bowman's space and capillary tufts with patent lumina that was covered by podocytes (Figures 8 A,B). Proximal tubules with their lining cells consisted of basally located euchromatic nuclei. The tubular cells rested on basement membrane while their apical part showed microvilli. The tubular cytoplasm contained basal elongated mitochondria and electron dense lysosomes (Figure 8C).

**Group II** (CCl4-treated group): Glomerulus covered by podocyte with its horse shoe nucleus and effacement of its foot processes. The capillaries were lined by endothelial cells and their lumina contained electron lucent material (Figure 9A). Some cortical tubules showed electron lucent cast in their lumina. Other tubules showed eroded surface and numerous vacuoles as well as lysosomes (Figure 9B). The cells of the proximal convoluted tubules had heterochromic nuclei and vacuolated cytoplasm together with partial loss of their brush borders. PCT contained irregular shape and disrupted mitochondria (Figure 9C).

**Group III** (CCl4 + CoQ10 treated group): Glomerulus with patent glomerular capillaries contained podocyte with its primary process, foot processes and patent filtration slits were seen (Figure 10A). PCT with basally located

euchromatic nuclei were detected. The tubular cells rested on basal lamina and the cytoplasm contained lysosomes and vacuoles. Intact apical brush border was seen (Figure 10B).

**Morphometric and statistical results**

Highly statistically significant increase in area percentage of collagen fiber deposition and iNOS respectively were seen in CCL4 administered group relative to control group, and COQ10-treated group. Meanwhile, non-significant difference between COQ10-administered group and in control group were noticed in all these parameters (Table 1, Histograms 1,2).

**Biochemical Results**

The biochemical investigations showed highly statistically significant elevation in the mean serum creatinine and BUN levels in CCL4 –administered group versus control group, and COQ10 –administered group. However, there was statistically non-significant difference between control group and COQ10 administered group in all these parameters (Table 2, Histograms 3,4).

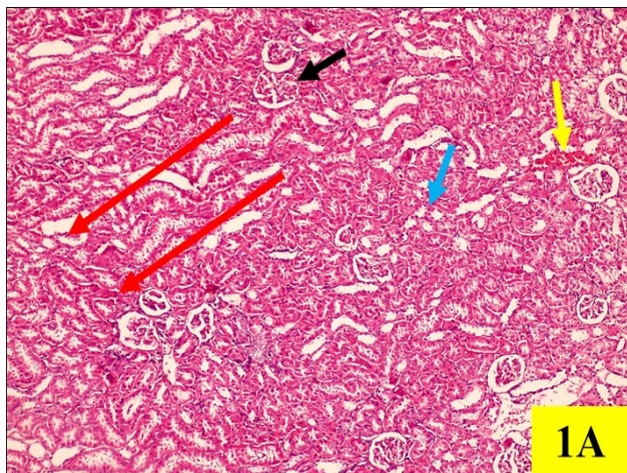


**Fig. 1A:** A photomicrograph of a section of the renal cortex of rats of group I (control group) showing the renal cortex formed of renal corpuscles (black arrow), proximal and distal convoluted tubules (blue arrow) and blood vessel (yellow arrow). Notice straight tubules originating from the medulla toward the cortex (medullary rays) (red arrow). (H&E x200)

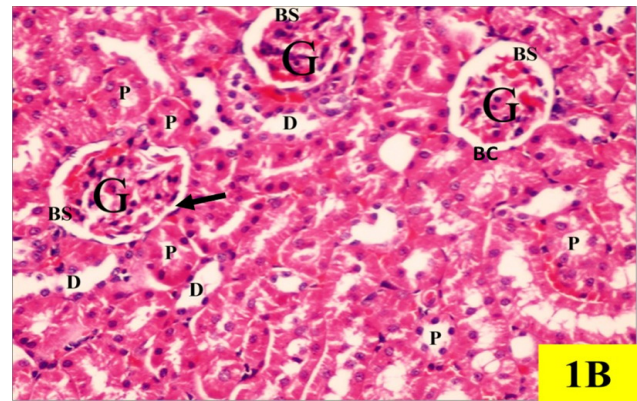


**Fig. 1B:** A photomicrograph of a section of the renal cortex of rats of group I (control group) showing renal corpuscles formed of glomerular (G) tuft of capillaries and Bowman's capsule (BC). Bowman's capsule is formed of outer parietal layer (black arrow) and inner visceral layer. The parietal layer consists of simple squamous epithelium resting on basement membrane. Bowman's capsule (BC) encloses space called Bowman's space (BS) between parietal layer and inner visceral layer. Notice the proximal convoluted tubules (P) and the distal convoluted ones (D). (H&E x400)

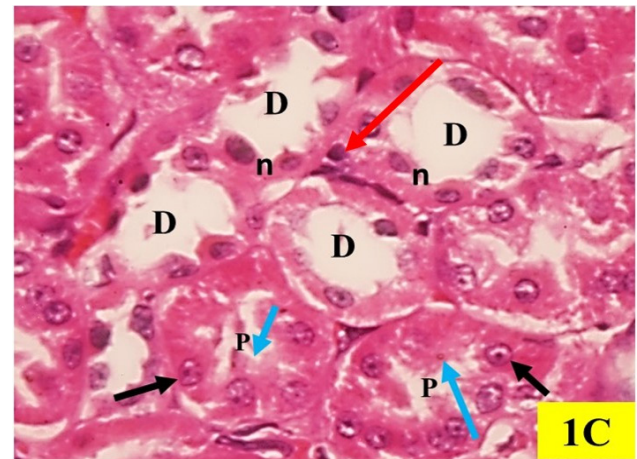


**Fig. 1C:** A photomicrograph of a section of the renal cortex of rats of group I (control group) showing the proximal convoluted tubules (P) with narrow lumina lined by tall columnar acidophilic epithelial cells with basally situated rounded nuclei (black arrow). Notice the presence of a prominent apical brush border (blue arrows). The distal convoluted tubules (D) have wider lumina and are lined by low cuboidal epithelium with apically situated nuclei (n). Notice, the nuclei of the interstitial cells of the renal cortex (red arrow). (H&E x1000)

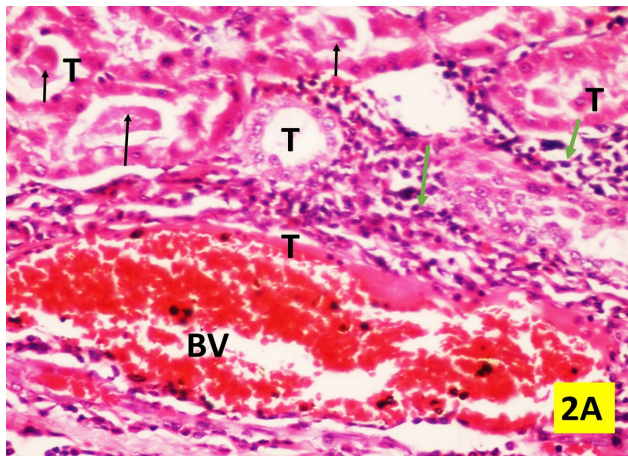


**Fig. 2A:** A Photomicrograph of section of the renal cortex of rats of group II (CCL4-treated group) showing wide interstitial spaces containing congested and dilated blood vessels (BV), together with perivascular and peritubular mononuclear inflammatory cell infiltrate (green arrows). Notice hyaline and cellular casts (Black arrow) in the lumina of the tubules (T). (H&E x400)

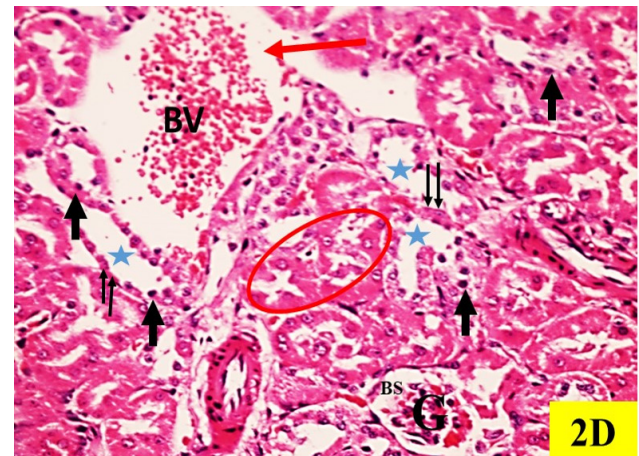


**Fig. 2D:** A photomicrograph sections of the renal cortex of rats of group II (CCL4-treated group) showing distortion of the arrangement of the convoluted tubules, with loss of clear demarcation between adjacent tubules (red circle). Some tubules show dilatation (stars) with flattening of their lining epithelium (double arrow). Other tubular cells show small pyknotic nuclei (black arrows). G= glomerulus, BS= Bowman's space. Notice rupture of the capillaries (BV) with interstitial hemorrhage (red arrows). (H&E x1000)

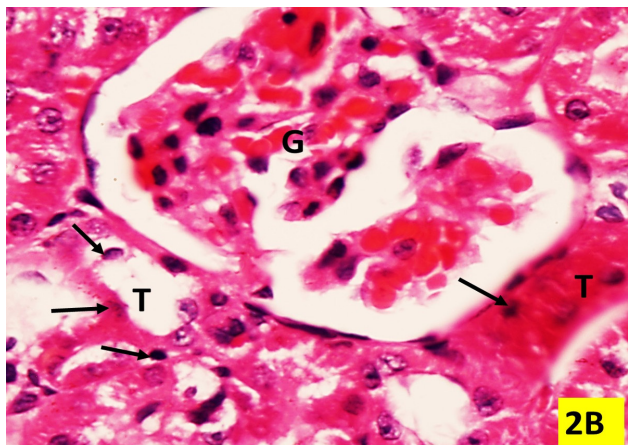


**Fig. 2B:** A photomicrograph of sections of the renal cortex of rats of group II (CCL4-treated group) showing congested glomerular (G) capillaries. Notice, the denuded tubules (T) with nuclear pyknosis & karyolysis (black arrow). (H&E x1000)

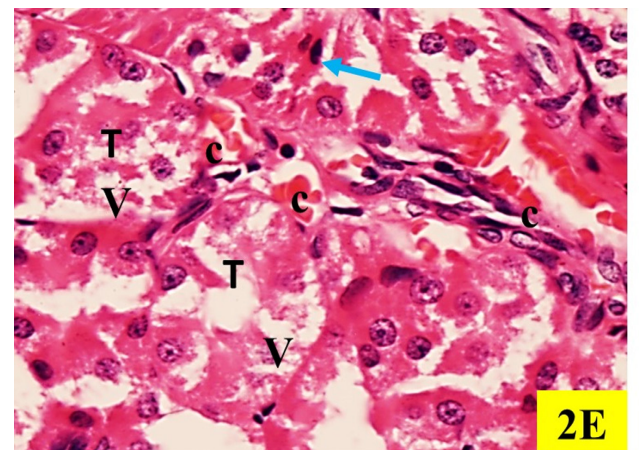


**Fig. 2E:** A photomicrograph of sections of the renal cortex of rats of group II (CCL4-treated group) showing cytoplasmic vacuolations (V) of tubular cells (T). Some tubules reveal denuded and exfoliated cells into the tubular lumina (blue arrow). Notice the congested peritubular capillaries (c). (H&E x1000)

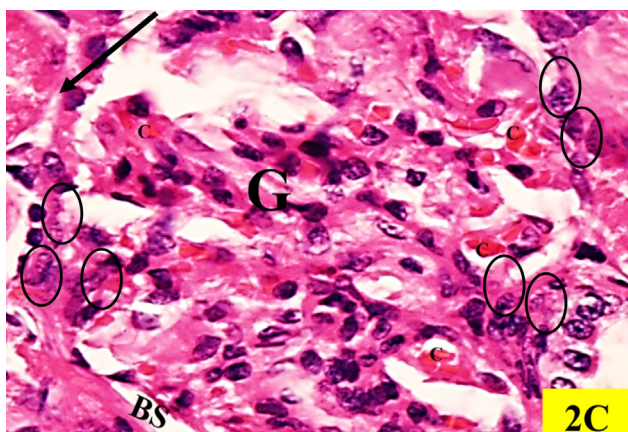


**Fig. 2C:** A photomicrograph of sections of the renal cortex of rats of group II (CCL4-treated group) showing hypercellularity of the glomerulus (G) with obliteration of Bowman's space (BS). Adhesion (black arrow) of capillary tuft to the parietal layer the Bowman's capsule is detected. Numerous cells (black circle) with pale nuclei can be seen in the parietal layer of Bowman's capsule and glomerular capillaries (c). (H&E x1000)

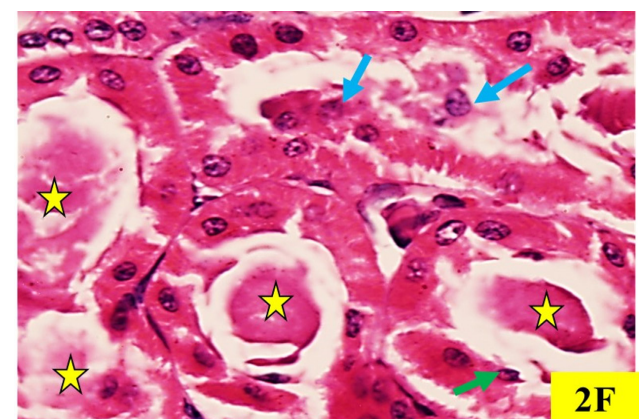


**Fig. 2F:** A photomicrograph of sections of the renal cortex of rats of group II (CCL4-treated group) showing some tubules with intraluminal hyaline casts (yellow stars) and degenerated nuclei (green arrow). Some tubules show separation of their epithelium from basement membrane with exfoliation of their lining cells (blue arrows). (H&E x1000)

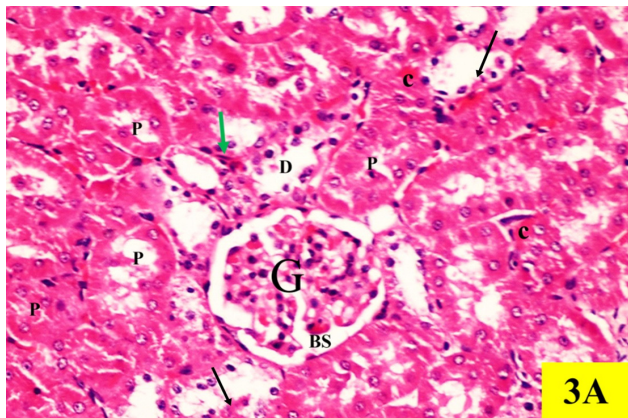


**Fig. 3A:** A photomicrographs of sections of the renal cortex of rats of group III (CCL4 + CoQ10-treated group) showing normal renal corpuscle. A glomerulus (G) is surrounded by distinct Bowman's space (BS). Some proximal (P) and distal (D) convoluted tubules appear normal. But other tubules show degenerative changes (green arrow). Notice: the presence of hyaline castes inside the lumina of some tubules (black arrow).(H&E x 400)

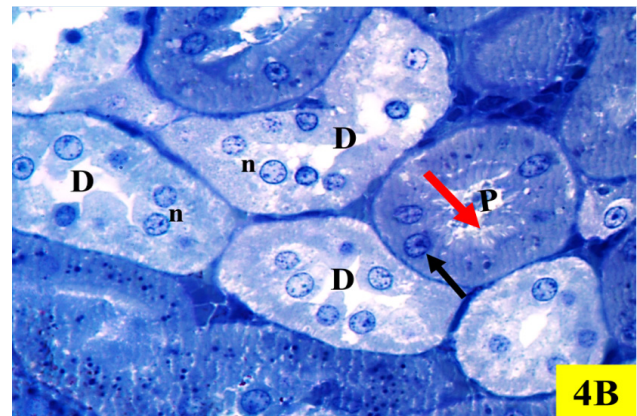


**Fig. 4B:** A photomicrograph of semi thin sections of the renal cortex of (Control group) showing proximal convoluted tubule (P) lined with tall dark columnar cells with basally situated vesicular rounded nuclei (black arrow) and characteristic apical brush border (red arrow). The distal convoluted tubules (D) are lined with low cuboidal cells with apically situated nuclei (n) and pale stained cytoplasm. (Toluidine blue x 1000)

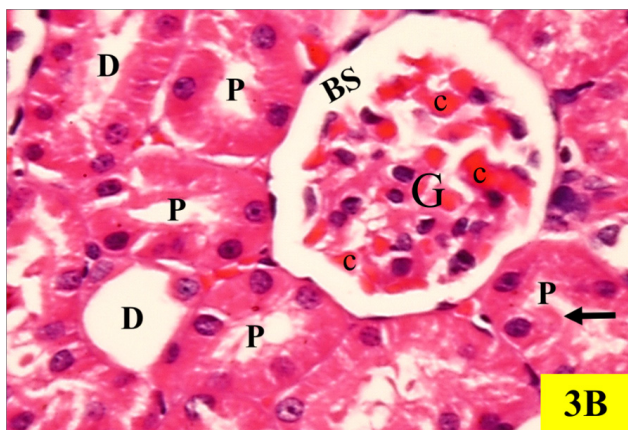


**Fig. 3B:** A photomicrograph of sections of the renal cortex of rats of group III (CCL4 + CoQ10-treated group) showing normal appearance of renal corpuscle, glomerular capillaries (c) and Bowman's space(BS). Notice the proximal (P) and distal (D) convoluted tubules, and the preserved brush borders (arrow) of the proximal convoluted tubules (P). (H&E x1000)

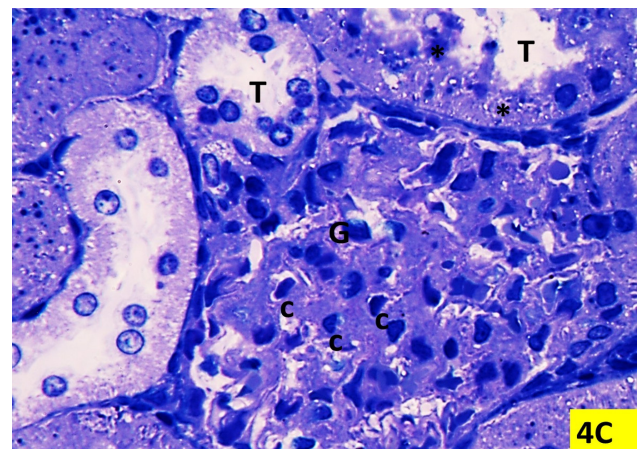


**Fig. 4C:** A photomicrograph of semi thin sections of the renal cortex of (CCL4-treated group) showing hypercellularity of the glomerulus (G), with congested glomerular capillaries (c) and obliteration of Bowman's space. Some tubules (T) show denuded surface and exfoliated nuclei (\*). (Toluidine blue x 1000).

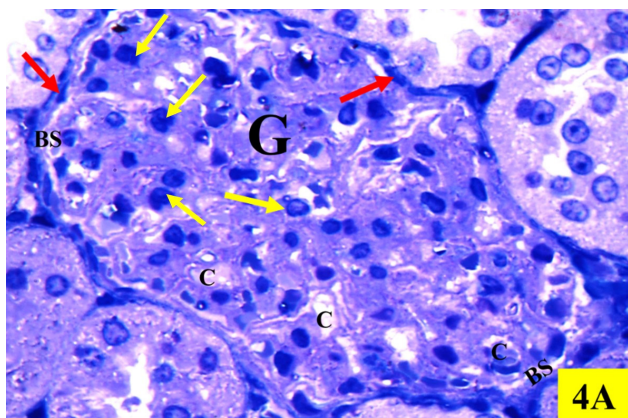


**Fig. 4A:** A photomicrograph of semi thin sections of the renal cortex of (control group) showing renal corpuscle and tubules. Renal corpuscle is formed of The parietal layer of Bowman's capsule lined by a single layer of flattened squamous epithelium (red arrows). Visceral layer appears in the form of cells with large nuclei (yellow arrow) covering the patent glomerular(G) capillaries (C). BS =Bowman's space. (Toluidine blue x1000)

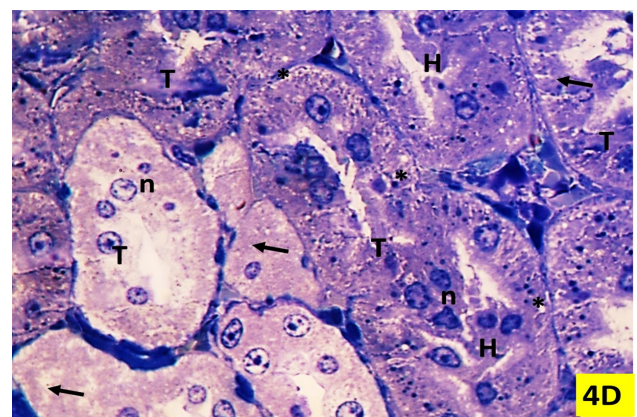


**Fig. 4D:** A photomicrograph of semi thin sections of the renal cortex of (CCL4-treated group) showing the convoluted tubules (T) with denuded surface (black arrow) and multiple casts (H) in their lumina. Notice tubular vacuolations (\*) and exfoliated nuclei inside the lumen of the tubules(n). (Toluidine blue x 1000).

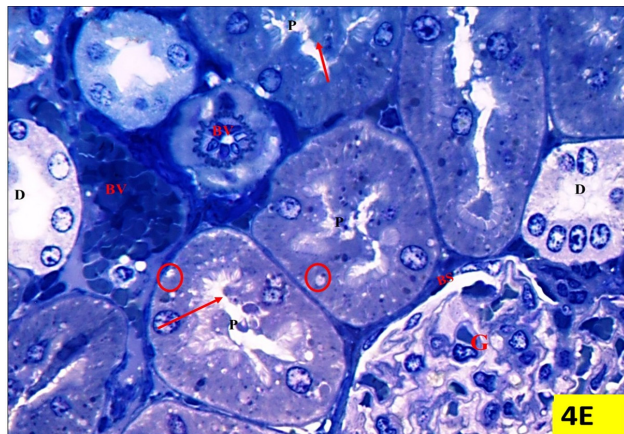


**Fig. 4E:** A photomicrograph of semi thin sections of the renal cortex of (CCL4 + CoQ10 -treated group): showing normal renal corpuscle with patent glomerular capillaries(G) & patent Bowman's space (BS). The proximal convoluted tubules (P) are lined by columnar cells with brush border and basally situated vesicular nuclei (red arrow). Distal convoluted tubules (D) appear normal. Few tubular cells showing vacuolated cytoplasm (red circles). Notice: interstitial congested blood vessels (BV). (Toluidine blue X 1000).

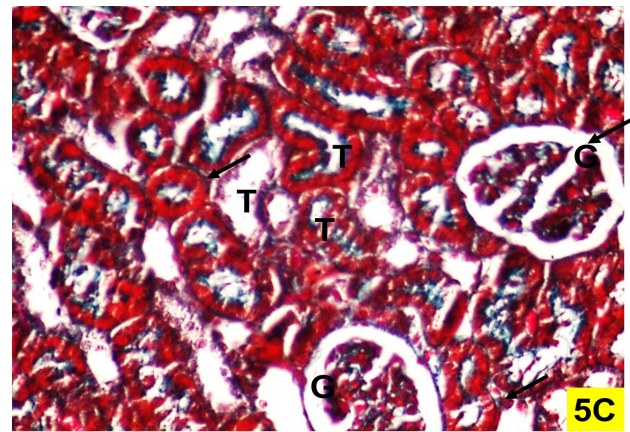


**Fig. 5C:** A photomicrograph of Masson's Trichrome stained sections in the renal cortex of (CCL4 + CoQ10 treated group) showing; few collagen fibers (arrow), deposition is found per glomerular(G) and peritubular (T). (Masson's Trichrome x 400).

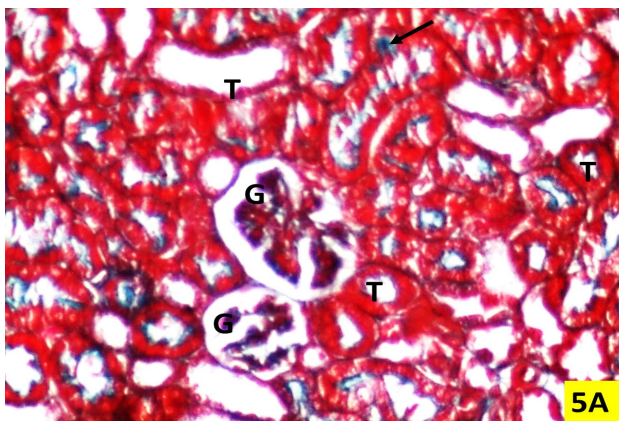


**Fig. 5A:** A Photomicrograph of Masson's Trichrome stained sections in the renal cortex of (Control group): showing thin minimal collagen fibers deposition (arrow) peri glomerular (G) and peri tubular (T). (Masson's Trichrome x 400).

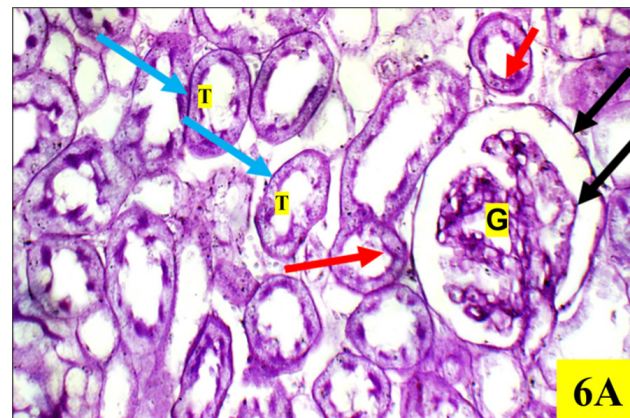


**Fig. 6A:** A photomicrograph of PAS stained sections in the renal cortex of (Control group) showing PAS positive reaction of basement membrane of the glomerular capillaries (G), and basement membrane of parietal layer of the Bowman's capsule (black arrows). All tubules (T) showing PAS positive basement membrane (blue arrow). PCT showing PAS positive apical brush borders (red arrows). (PAS x 400)

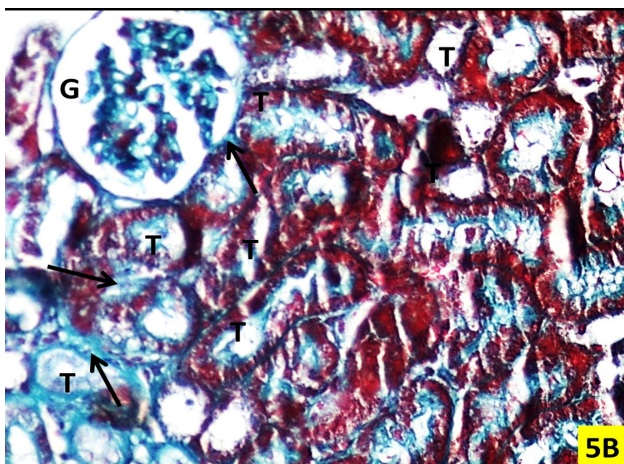


**Fig. 5B:** A photomicrographs of Masson's Trichrome stained sections in the renal cortex of (CCL4-treated group) showing marked increase in the collagen fibers (arrow) deposition can be detected peri glomeruli (G) and peri tubular (T). (Masson's Trichrome x 400).

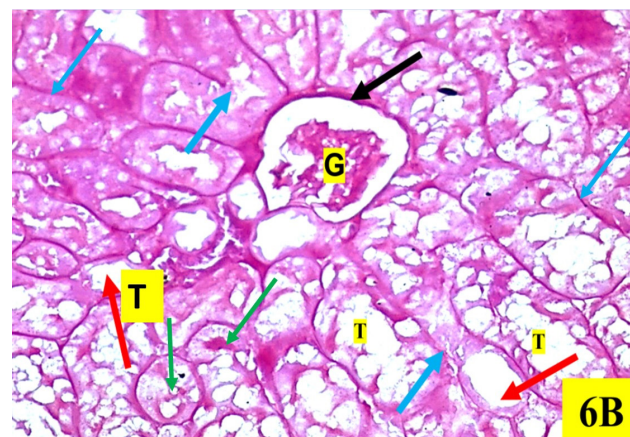


**Fig. 6B:** A photomicrograph of PAS stained sections in the renal cortex of (CCL4-treated group): showing apparent increase in the PAS positive reaction in the mesangial matrix and basement membrane of the glomerular capillaries and parietal layer of the Bowman's capsule (black arrow). All tubules showing apparent increase in the PAS positive basement membrane (blue arrows). Some tubules show PAS positive hyaline casts (green arrows). PCT show apparent decrease in PAS positive reaction of brush border (red arrows). (PAS x 400)

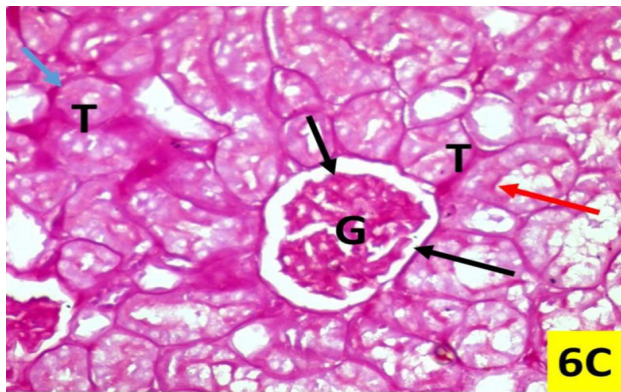


**Fig. 6C:** A photomicrograph of PAS stained sections in the renal cortex of (CCL4 + CoQ10 treated group): showing normal positive PAS reaction in the basement membrane of glomerular capillaries (G), Bowman's capsule (black arrows), and the renal convoluted tubules (blue arrows). The brush border of the proximal convoluted tubules (T) is preserved and show PAS positive reaction (red arrows). (PAS x 400).

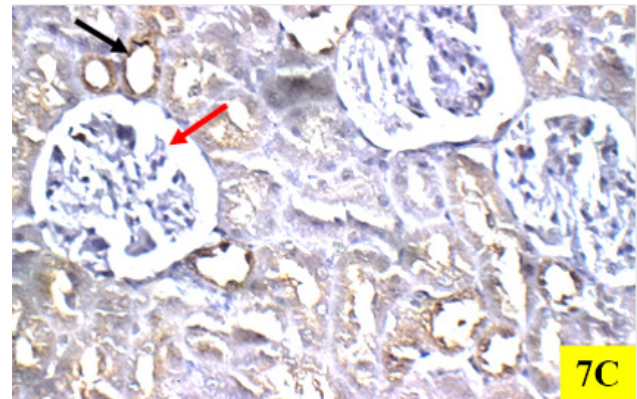


**Fig. 7C:** A photomicrograph of iNOS immunohistochemical stained sections in the renal cortex (CCL4 + CoQ10 treated group) showing negative cytoplasmic reactivity for iNOS in glomeruli (red arrow). Most of the tubules show weak iNOS (black arrow). (iNOS immunostain X 400)

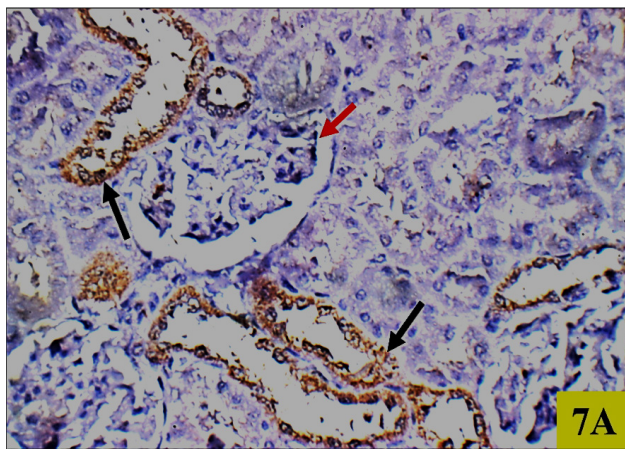


**Fig. 7A:** A photomicrograph of iNOS immunohistochemical stained sections in the renal cortex of (Control group) showing negative cytoplasmic reactivity in glomeruli. (red arrow). Weak cytoplasmic reactivity is detected in the proximal tubular cells (black arrow). (iNOS immunostain X 400)

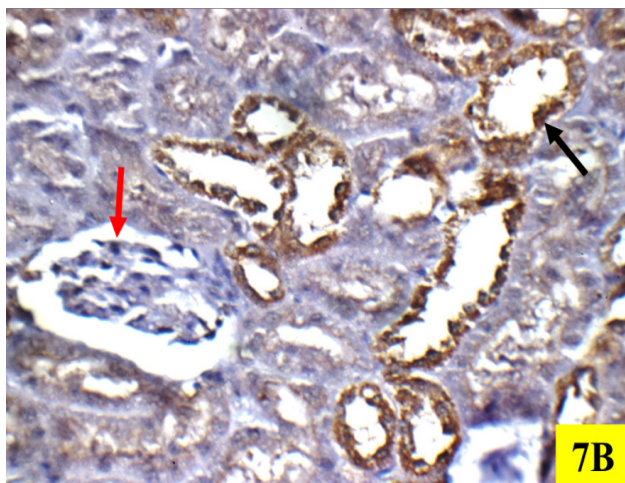


**Fig. 7B:** A photomicrograph of iNOS immunohistochemical stained sections in the renal cortex of (CCL4-treated group) showing negative cytoplasmic reactivity in glomeruli (red arrow), Some tubular cells show weak iNOS, other tubules show strong iNOS (black arrow). (iNOS immunostain X 400)

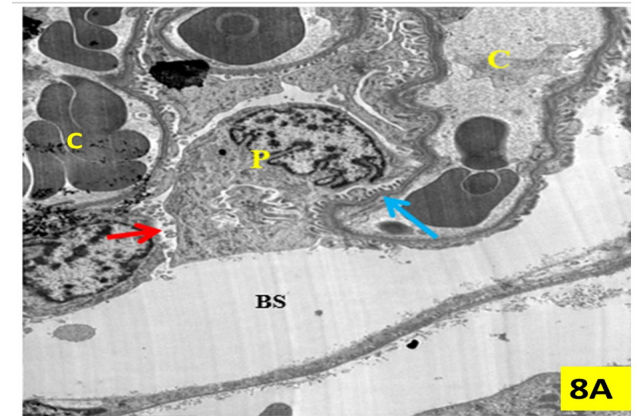


**Fig. 8A:** An electron micrograph of a section of the renal cortex of a rat of group I (Control group) showing part of renal corpuscle containing Bowman's space (BS). Glomerular capillary tufts show patent capillaries (C). The capillaries are covered by 2 podocytes (P) with foot process and patent filtration slits (blue arrow) (TEM x5000)

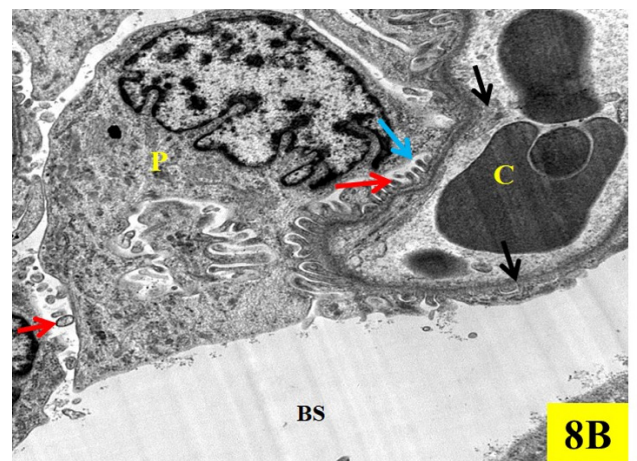


**Fig. 8B:** An electron micrograph of a section of the renal cortex of a rat of group I (Control group) showing part of renal corpuscle containing podocytes, Glomerular capillary tufts and Bowman's space (BS). Glomerular capillary tufts show patent capillaries (C) lined by endothelial cells (black arrow). The capillaries are covered by 2 podocytes (P) with foot process (red arrow) and patent filtration slits (blue arrow) (TEM x10000)

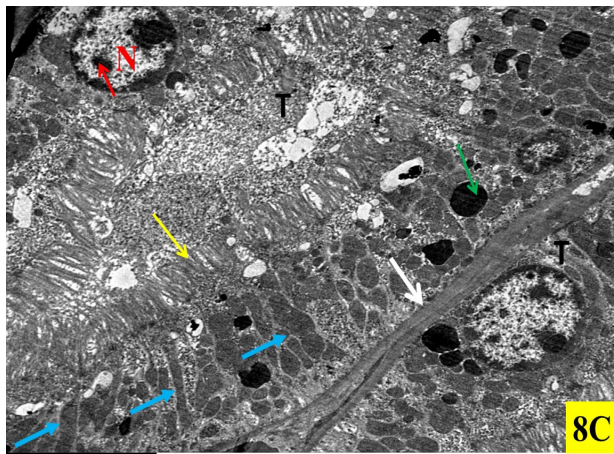


**Fig. 8C:** An electron micrograph of a section of the renal cortex of a rat of group I (Control group) showing part of 2 proximal tubules (T) with their lining cells consist of basally located euchromatic (red arrow) nuclei (N). The cells rest on basement membrane (white arrow) while apical part shows microvilli (yellow arrow). The cytoplasm contains basal elongated mitochondria (blue arrow) and electron dense lysosomes (green arrow). (TEM x 5000)

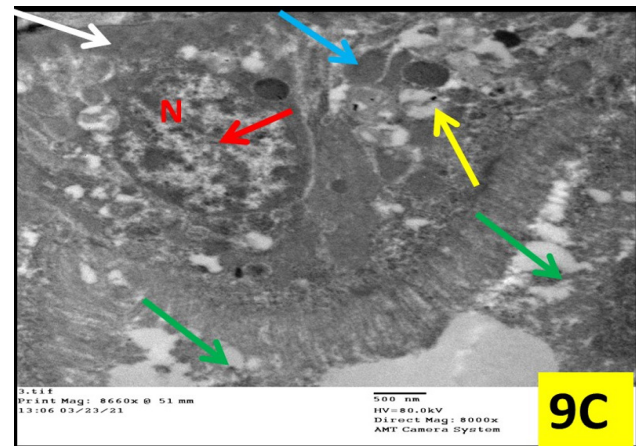


**Fig. 9C:** An electron micrograph of a section of the renal cortex of a rat of group II (CCl4-treated group) showing part of proximal convoluted tubules cells resting on basal lamina (white arrow). The nuclei (N) has clumped heterochromatin (red arrow). The cytoplasm has vacuolations, (yellow arrow) and irregular shape & disruption of the mitochondria (blue arrow) and partial loss of brush border (green arrow). (TEM X 8660)

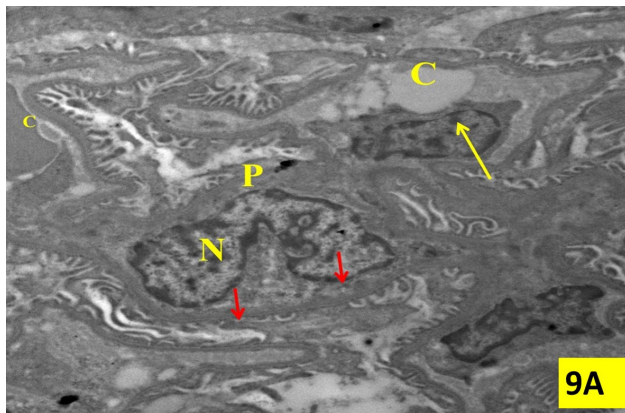


**Fig. 9A:** An electron micrograph of a section of the renal cortex of a rat of group II (CCl4-treated group) showing part of glomerulus covered by podocyte (P) with bizarre shaped nucleus (N) and effacement of foot processes (red arrow). The capillaries (C) are lined by endothelial cells (yellow arrow) and their lumina contain electron lucent material. (TEM x 8660)

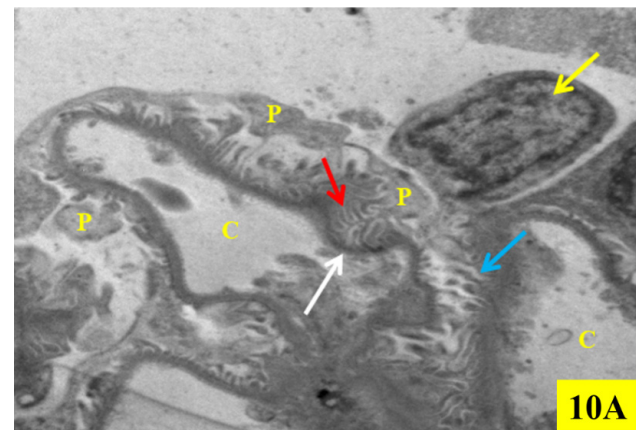


**Fig. 10A:** An electron micrograph of a section of the renal cortex of a rat of group III (CCl4 + CoQ10 treated group) showing part of glomerulus containing podocyte (yellow arrow) with its primary process (p), foot processes (red arrow) and patent filtration slits (blue arrow). Notice patent glomerular capillaries (C) with basement membrane (white arrow). (TEM X 8660)

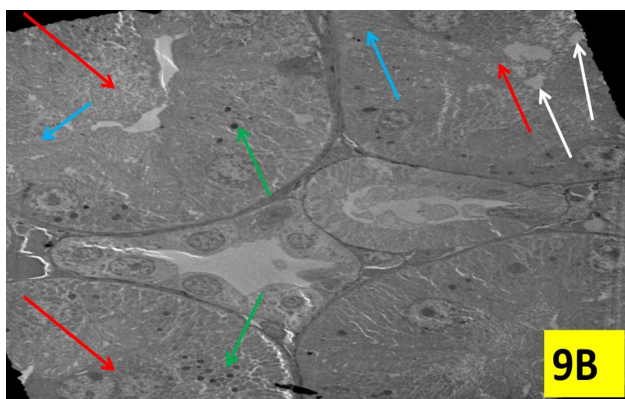


**Fig. 9B:** An electron micrograph of a section of the renal cortex of a rat of group II (CCl4-treated group) showing some cortical tubules (T) with hyaline cast (red arrow) in the lumen. Some tubules show denuded surface (karyolysis) with loss of nuclei (blue arrow), numerous vacuoles (white arrow) and lysosomes (green arrow). (TEM x 1620)

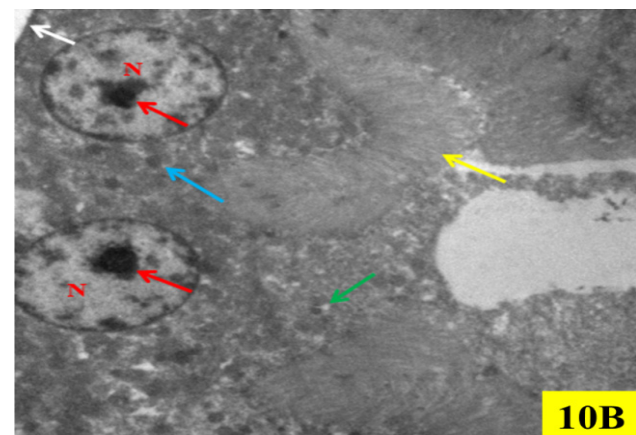


**Fig. 10B:** An electron micrograph of a section of the renal cortex of a rat of group III (CCl4 + CoQ10 treated group) showing part of PCT with basally located nuclei (N) that is euchromatic (red arrow). The tubules cells rest on basal lamina (white arrow) and the cytoplasm contain lysosomes (blue arrow) and vacuoles (green arrow). Notice intact apical brush border (yellow arrow). (TEM x 5410).

**Table 1:** Comparing the area percentage for collagen fiber deposition and the area percentage for iNOS among the three study groups

Parameters	Control group I	Group II (CCL4-treated group)	Group III (CCL4+CoQ10-treated group)	Test value	P-value
Area percent of brown color (cytoplasmic iNOS) Mean±SD	0.051 ± 0.01	0.28 ± 0.03	0.07 ± 0.03	204.004	<0.001**
Area percent of green color (%) (collagen deposition) Mean±SD	13.23 ± 4.89	53.23 ± 10.25	17.60 ± 6.99	64.973	<0.001**
Post Hoc analysis					
		Group I Vs Group II	Group I Vs Group III		Group II Vs Group III
Area percent of brown color (cytoplasmic iNOS)		<0.001**	0.111*		<0.001**
Area percent of green color (%) (collagen deposition)		<0.001**	0.169*		<0.001**

P-value >0.05: Non significant (NS); P-value <0.05: Significant (S); P-value < 0.01: highly significant (HS)

•: One Way ANOVA test.

\*\* : Highly significant

\*: Non-significant

**Table 2:** Comparing the serum creatinine & BUN levels among the three study groups

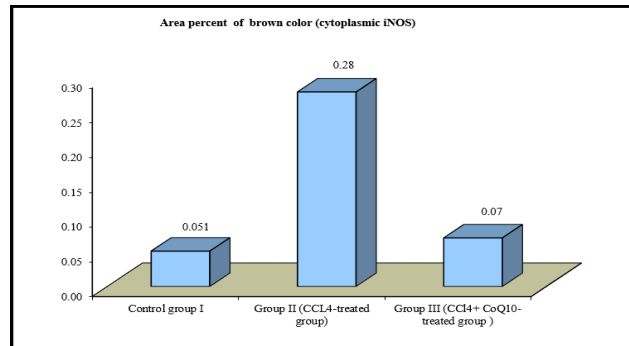
Parameters	Control group I	Group II (CCL4-treated group)	Group III (CCL4+CoQ10-treated group)	Test value	P-value
Serum creatinine (mg/dl) Mean+/-_SD	0.42 ± 0.079	0.80 ± 0.01	0.50 ± 0.08	75.598	<0.000**
Serum BUN (mg/dl) Mean+/-_SD	18.97 ± 0.65	29.01 ± 1.11	19.23 ± 0.96	305.128	<0.000**
Post Hoc analysis					
		Group I Vs Group II	Group I Vs Group III		Group II Vs Group III
Serum creatinine		<0.001**	0.064*		<0.001**
Serum BUN		<0.001**	0.536*		<0.001**

P-value >0.05: Non significant (NS); P-value <0.05: Significant (S); P-value < 0.01: highly significant (HS)

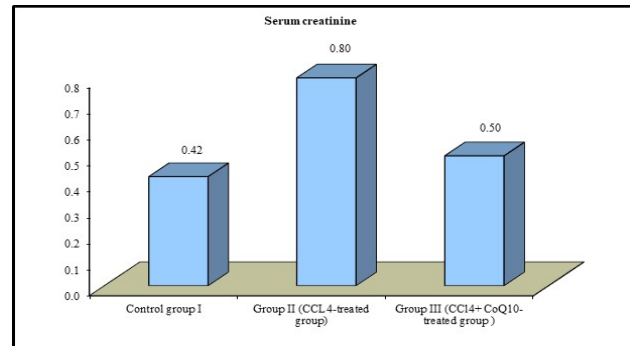
•: One Way ANOVA test.

\*\* : Highly significant

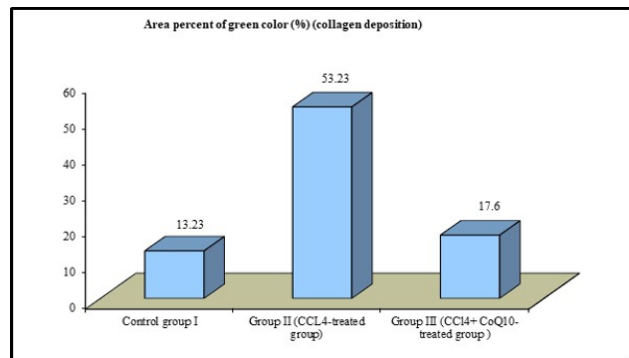
\*: Non-significant



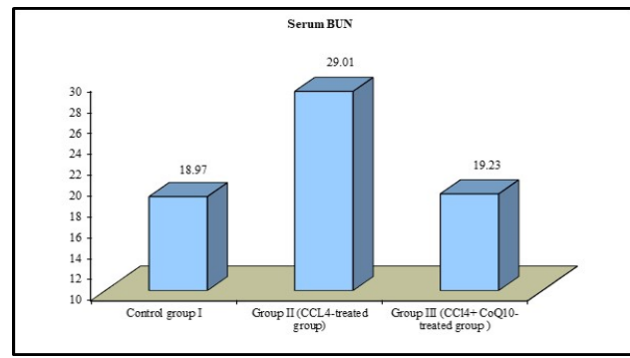
**Histogram 1:** Demonstrating the comparison between the three groups as regards area percent of the brown color (cytoplasmic iNOS).



**Histogram 3:** Demonstrating the comparison between the three groups as regards the serum creatinine.



**Histogram 2:** Demonstrating the comparison between the three groups as regards the area percent of green color (%) (collagen deposition).



**Histogram 4:** Demonstrating the comparison between the three groups as regards the serum BUN.

## DISCUSSION

CCl<sub>4</sub> has many hazards being a toxin. CCl<sub>4</sub> produces oxygen free radicals in some organs leads to their toxicity such as the hepatic, renal, pulmonary, cerebral, and hematological toxicity<sup>[18]</sup>. CCl<sub>4</sub> is used in animal models to induce nephrotoxicity as it affects the renal tubules, glomeruli, and interstitial tissue. Previous studies reported that it is concentrated in a large amount in the cortex of the kidney specifically<sup>[19]</sup>.

In the present study, LM examination of the H&E stained sections of group II revealed expansion of the glomerular capillary tuft with adhesions between it and its capsule of Bowman.

EM examination of the same group showed abnormal shaped podocytes with horseshoe nuclei and effacement of foot processes. Moreover, some studies reported that change of cytoskeleton of podocyte was a common reaction following injury<sup>[20]</sup>. Expansion of podocytes occurred due to decrease their number relative to glomerular volume. Kriz, *et al.* (2013) added, mechanical force on podocyte leads to downregulation of integrin that link podocyte to the glomerular basement membrane (GBM)<sup>[20]</sup>. Also, other workers stated that if injury of the podocyte was severe, it might detach from GBM allowing adhesions between glomerular capillaries and parietal layer of capsule of Bowman and consequently glomerular sclerosis<sup>[21]</sup>. Moreover, other authors declared that increase secretion of TGFβ from damaged tubules and inflammatory cells leads to decrease in integrin expression and subsequent loss of podocyte adhesion to the glomerular capillary and podocyte death<sup>[22]</sup>.

In the current work, the H&E stained sections showed that CCl<sub>4</sub> group showed hypercellularity of the glomeruli. This result was attributed to the presence of numerous pale stained cells, most properly originated from parietal layer of capsule of Bowman and migrated to glomerular tuft of capillaries. Recently, new studies reported the presence of stem cells in the parietal layer of Bowman's capsule that underwent proliferation & migration to replace the apoptotic podocytes<sup>[23]</sup>.

In the present study, examination of the Masson's trichrome stained sections showed deposition of type I collagen inside the glomerular capillary was detected in group II. This was explained by other study which declared that over expression of TGFβ induces synthesis of type I collagen by mesangial cells<sup>[22]</sup>.

One of the pathways and techniques of survival of cell and fighting against cell death is autophagy<sup>[24]</sup>. Normal autophagy regulates the turnover of collagen. It maintains the structure and function of the kidney<sup>[24]</sup>. The glomerular injury is attributed to dysregulation of autophagy Tang *et al.* (2020) added, under oxidative stress, due to CCl<sub>4</sub>, autophagy is altered with a subsequent excessive collagen deposition and inhibition of collagen degradation<sup>[24]</sup>.

The mechanism by which CCl<sub>4</sub> induced lipid peroxidation of many structures occur under the effect of its metabolite the trichloromethyl (CCl<sub>3</sub>), free radicals that is formed from reaction between CCl<sub>4</sub> and liver cytochrome P450<sup>[5]</sup>. (CCl<sub>3</sub>) in the presence of oxygen, trichloromethyl peroxy radical (CCl<sub>3</sub>O<sub>2</sub>) is produced, which is highly injurious<sup>[25]</sup>. When these damaging radicals combined with DNA, proteins and lipids cause severe cell injury<sup>[26]</sup>. This cell injury is resulted from the increase of permeability of the plasma membrane, endoplasmic reticulum and mitochondria. This may result in an alteration of calcium regulation and consequently cell necrosis<sup>[27]</sup>. Moreover, CCl<sub>4</sub> decreases antioxidants concentration in tissues that render them liable to severe structural dysfunction<sup>[28,29]</sup>.

In the present study, the LM examination of the H&E stained sections showed that rats received CCl<sub>4</sub> revealed marked affection & distortion of the normal cortical architecture. The renal tubules appeared to be very sensitive to CCl<sub>4</sub> toxicity, and this was particularly confirmed also by the PAS and ultrastructural examination. The convoluted tubules showed sever deviation from normal structure. Most of the tubules showed dilatation with degeneration of their lining epithelium with vacuoles in the cytoplasm. Small dark stained nuclei noticed in most of the nuclei. The eroded surface of the tubules was most probably due to the diminished integrin<sup>[30,31]</sup>.

In this study, PAS stained sections of the CCl<sub>4</sub>- treated group II showed destructed brush borders of PCT due to ischemic changes. Some of the tubules showed lumina filled with exfoliated nuclei and hyaline casts. These findings were confirmed by statistically highly significant increment of the area % of iNOS reactivity in the PCT relative to the control group. This was in accordance with Alayunt *et al.* (2019)<sup>[30]</sup>. Alayunt *et al.* (2019) demonstrated that oxidative stress and inflammation markers were significantly higher in CCl<sub>4</sub> administered rat group<sup>[30]</sup>. The results of PAS stained sections were explained by Klatt *et al.* 2022<sup>[31]</sup>, they added that the injury of the PCT leads to disturbance and decrease in the blood flow. Ischemic changes cause many histological changes in the lining cells with subsequent disturbed polarity of the cells of the PCT. This leads to redistribution of the membrane bound proteins (like Na<sup>+</sup>K<sup>+</sup> ATPase enzyme) which become shifted from the basolateral layer of the tubular cells to the opposite aspect (brush border) of cells near the lumen<sup>[31]</sup>. This may result in a decrease of the sodium reabsorption by proximal tubules and hence high concentrated intraluminal solute will be delivered to the distal convoluted tubules and then through a tubulo-glomerular feedback system<sup>[31]</sup>. The excess of sodium in the macula densa causes its swelling and triggers it to release renin which will lead to vasoconstriction of the glomerular capillaries and the nearby afferent arterioles resulting into reduction in the filtration rate of the glomeruli<sup>[31]</sup>. Moreover, Klatt *et al.* 2022<sup>[31]</sup>, added that loss of connection between the renal tubular cells and their basement membranes leads to their falling into the urine and subsequent formation of

cellular and hyaline casts in the tubular lumen. This occurs due to changes of integrin that are connected to tubular cells<sup>[31]</sup>. So, the cellular and hyaline casts in the tubular lumen most likely block the outflow of urine leading to an increase in the intratubular pressure which also decreases the GFR. The decrease in GFR is a compensatory protective mechanism to decrease the sodium load, allowing more time for sodium resorption because the flow become slower<sup>[31]</sup>.

In the active study, the H&E stained sections of the CCL4- treated group revealed wide interstitial spaces containing congested and dilated thick-walled blood vessels and mononuclear inflammatory cell infiltrate. Also, peritubular and periglomerular collagen fibers deposition were confirmed by statistically highly significant increase in the area % collagen fibers deposition. These results agreed with some studies stating that, inflammatory responses are associated with recruitment of neutrophils, macrophages, and lymphocytes<sup>[32]</sup>. Moreover, others added that TNF- $\alpha$  and IL-1, are inflammatory cytokines that are produced by the activate macrophages which increase the number of fibroblasts<sup>[12,33]</sup>.

In this study, the H&E stained sections of the CCL4 -treated group revealed damaged endothelial cells with subsequent interstitial hemorrhage. This finding is in agreement with<sup>[34]</sup>. These results were due to injured tubules which produce fluid that may escape into the interstitium increasing interstitial pressure that are ultimately causing tubular compression and occlusion. Additionally, they stated that the ischemic tubular cells produce adhesion molecules like P-selectin that attract neutrophils and macrophages that contribute to more tissue damage (interstitial inflammation)<sup>[31]</sup>.

In several previous studies, the antioxidant coenzyme Q10 (CoQ10) was tested to mitigate the CCl4-induced hepatotoxicity and cardiotoxicity, however its effect on nephrotoxicity has not yet been clarified. Several antioxidant chemicals have been suggested as preventive medicines against CCl4-induced nephrotoxicity. Furthermore, there is considerable debate around CoQ10's nephroprotective potentiality. This prompted us to investigate CoQ10's potential to protect the kidneys from the cortical damage caused by CCl4<sup>[35]</sup>. Coenzyme Q10 (CoQ10), a mitochondrial isoprenoid, is a fat-soluble vitamin like endogenous component. It has gained much popularity because of its medicinal value as a dietary supplement, immune booster, and antiaging<sup>[35]</sup>.

In the active study, group III (CCl4 + CoQ10-treated group) retained renal cortical structure almost normal. These results are in harmony with other workers who attributed the beneficial effect of CoQ10 versus CCl4-induced liver damage to the potential anti-inflammatory, antioxidant and anti-apoptotic properties of CoQ10<sup>[36]</sup>.

Interestingly, Yubero *et al.* (2016) reported that, CoQ10 prevented CCl4 conversion into its reactive toxic metabolites like (CCl3) and (CCl3OO) radicals. They also

added that CoQ10 protected hepatic antioxidant enzymes activities and remove oxygen free radical<sup>[37]</sup>.

In the current work, simultaneous administration of CoQ10 with CCl4 showed anti-inflammatory activity. This agreed with other studies that demonstrated the anti-inflammatory effect of CoQ10<sup>[38]</sup>. It was stated that CoQ10 decreases production of pro-inflammatory cytokines and thus possess anti inflammatory properties<sup>[26,39]</sup>.

In the present study, co-administration of CoQ10 with CCl4 showed anti-fibrotic effect. Group III (CCL4 + CoQ10 treated group) revealed few deposition of collagen fibers in the peritubular, periglomerular and interstitial areas. Statistically, it showed highly significant reduction of in the area % of green color. This finding is in accordance with other studies which, revealed that CoQ10 showed an anti-fibrotic activity in the renal tissue in rats<sup>[38]</sup>. Moreover, this effect is attributed to the ability of CoQ10 to suppress the synthesis of TGF- $\beta$ 1<sup>[40]</sup>. In addition, CoQ10 has shown significant increase in the antioxidant markers and decrease in the oxidative markers<sup>[41]</sup>.

In this work, the area % of iNOS immunoreactivity of group III (CCl4 + CoQ10-treated group) showed statistically highly significant decrease. These findings agree with those who also found the decrease in the immunoreaction for iNOS in both the control and CoQ10-treated groups<sup>[13]</sup>. The CoQ10 showed anti-genotoxic effect and modulating the expression of gene responsible for iNOS synthesis in colonic mucosa in rats<sup>[42]</sup>. Furthermore, recently it was demonstrated that CoQ10 decreases production of ROS due to its anti-inflammatory and immuno-modulatory action<sup>[43]</sup>.

In the present study, CoQ10 was of great benefit on lowering peroxidation of lipids. Its administration in group III ameliorated the oxidative renal injury produced by CCl4 administration in group II and normalized the serum levels of kidney function biomarkers (serum BUN and creatinine)<sup>[23]</sup>. In addition, it was noted that the CoQ10 is associated with preservation of both cytochrome P450 content and glutathione metabolizing enzymes<sup>[44,45,46]</sup>. Thus, CoQ10 exerted a protective effect against CCl4 induced damage to renal cortex via possessing anti-inflammatory, anti-fibrotic and antioxidant properties.

## CONCLUSION

CCl4 induced hazardous effects on the renal cortical structure with subsequent kidney functional impairment. On the other hand, CoQ10 showed a marked nephroprotective role in preventing or at least ameliorating the CCl4-induced renal toxicity. Thus, CoQ10 administration would be of great help in protecting against the hazardous effects of CCl4 on the renal tissue.

## CONFLICT OF INTERESTS

There are no conflicts of interest.

## REFERENCES

1. Akram, M., Manju Tembhre, M., Jabeen, R., Khalid, S., Sheikh, M., Jan, A., Farooq, U., & Amin, M. Defensive role of *Rosmarinus officinalis* in carbon tetrachloride-induced nephrotoxicity and oxidative stress in rats. *Bulletin of the National Research Centre*, 2019; 43: 50-60.
2. Safhi, M. Nephroprotective Effect of Zingerone against CCl<sub>4</sub>-Induced Renal Toxicity in Swiss Albino Mice: Molecular Mechanism. *Oxidative Medicine and Cellular Longevity*, 2018; 1-7.
3. Manibusan, M.K., Odin, M., & Eastmond, D.A. Postulated carbon tetrachloride mode of action: a review. *Journal of Environmental Science and Health. Part C, Environmental Carcinogenesis & Ecotoxicology Reviews*, 2007; 25(3): 185-209.
4. Yoshioka, H., Usuda, H., Fukuishi, N., Nonogaki, T., & Onosaka, S. Carbon tetrachloride-induced nephrotoxicity in mice is prevented by pretreatment with zinc sulfate. *Biol Pharm Bull.*, 2016; 39(6): 1042–1046.
5. Abd Elbaky, N., El-Orabi, N., Fadda, L., Abd-Elkader, O., & Ali, H. Role of N-Acetylcysteine and Coenzyme Q10 in the Amelioration of Myocardial Energy Expenditure and Oxidative Stress, Induced by Carbon Tetrachloride Intoxication in Rats. *Dose-Response: An International Journal*, 2018; 1-7.
6. Yousef, A., Fahad, A., Abdel Moneim, A., Metwally, D., El-khadragy, M., & Kassab, R. The Neuroprotective Role of Coenzyme Q10 Against Lead Acetate-Induced Neurotoxicity Is Mediated by Antioxidant, Anti-Inflammatory and Anti-Apoptotic Activities. *Int. J. Environ. Res. Public Health*, 2019; 16: 2895-2912.
7. Donnino, M.W., Cocchi, M.N., Saliccioli, J.D., Kim, D., Naini, A.B., Buettner, C., & Akuthota, P. Coenzyme Q10 levels are low and may be associated with the inflammatory cascade in septic shock. *Crit. Care*, 2011; 15: 189-197.
8. Villalba, J., Parrado, C., Santos-Gonzalez, M., & Alcain, F. Therapeutic use of coenzyme Q10 and coenzyme Q10-related compounds and formulations. *Expert Opinion on Investigational Drugs*, 2010; 19(4): 535-554.
9. Hernandez-Camacho, J.D., Bernier, M., Lopez-Lluch, G., & Navas, P. Coenzyme Q10 supplementation in aging and disease. *Front. Physiol.*, 2018; 9: 44-55.
10. Sohet, F., Neyrinck, A., Pachikian, B., de Backer, F., Bindels, L., Niklowitz, P., *et al.* Coenzyme Q10 supplementation lowers hepatic oxidative stress and inflammation associated with diet-induced obesity in mice. *Biochem. Pharmacol.*, 2009; 78(1): 1391–1400.
11. Pala, R., Beyaz, F., Tuzcu, M., Er, B., Sahin, N., Cinar, V., & Sahin, K. The effects of coenzyme Q10 on oxidative stress and heat shock proteins in rats subjected to acute and chronic exercise. *J Exerc Nutrition Biochem.*, 2018; 22(3): 14–20.
12. Hamam, G., Raafat, M., & Mostafa, H. Histological Study on Possible Therapeutic Effect of BM-MSCs on Healing of Lung Fibrosis Induced by CCl<sub>4</sub> with Reference to Macrophage Plasticity. *J Cytol Histol.*, 2019; 10(2): 537- 545.
13. Mazen, N., & Elnegris, H. Role of coenzyme Q10 in testicular damage induced by acrylamide in weaned albino rats: a histological and immunohistochemical study. *The Egyptian Journal of Histology*, 2013; 36:164-174.
14. Bancroft, J.D., & Layton, C. The hematoxylin and eosin, connective, and mesenchymal tissues with their stains. In: Suvarna SK, Layton C and Bancroft JD, editors. *Bancroft's theory and practice of histological techniques*. 7th edition. Churchill Livingstone: Philadelphia, 2013; 173- 212.
15. Abdel-Hady, E., & Abdel-Rahman, G. Protective effect of coenzyme Q10 on cadmium-induced testicular damage in male rabbits. *Am-Eurasian J Toxicol Sci.*, 2011; 3:153–160.
16. Bancroft, J.D., & Gamble, M. *Theory and practice of Histological techniques*, 6th ed. Churchill Livingstone, London, Elsevier, 2008; 377- 694.
17. Sawilowsky, S. Misconceptions leading to choosing the t test over the Wilcoxon Mann-Whitney U test for shift in location parameter. *Journal of Modern Applied Statistical Methods*, 2005; 4 (2): 598-600.
18. Yilmaz-Ozden, T., Can, A., Karatug, A., Pala-Kara, Z., Okyar, A., & Bolkent, S. Carbon tetrachloride-induced kidney damage and protective effect of *Amaranthus lividus* L. in rats. *Toxicology and Industrial Health*, 2016; 32(6): 1143-1152.
19. Jaramillo-juarez, F., Rodriguez-Vazquez, M.L., Rincon-Sanchez, A.R., Consolacion- Martinez, M., Ortiz, G.G., & Llamas, J. Acute renal failure induced by carbon tetrachloride in rats with hepatic cirrhosis. *Ann Hepatol.*, 2008; 7(4): 331–338.
20. Kriz, W., Shirato, I., Nagata, M., LeHir, M., & Lemley, K.V. The podocyte's response to stress: the enigma of foot process effacement. *Am J Physiol Renal Physiol.*, 2013; 304: 333-347.
21. Shankland, S., Smeets, B., Pippin, J., & Moeller, M. The emergence of the glomerular parietal epithelial cell. *Nat. Rev. Nephrol.*, 2014; 10: 158–173.
22. Ding Y & Choi ME. Regulation of autophagy by TGF- $\beta$ : emerging role in kidney fibrosis. *Semin Nephrol.*, 2014; 34(1):62-71.

23. Li ZH, Guo XY, Quan XY, Yang C, Liu ZJ, Su HY, An N, Liu HF. The Role of Parietal Epithelial Cells in the Pathogenesis of Podocytopathy. *Front Physiol.*, 2022; 13: 832772.
24. Lin, P., Chou, C., Ou, S., Fang, T., & Chen J. Review of Nutrition Supplements in Chronic Kidney Diseases: A GRADE Approach. *Nutrients*, 2021; 13: 469- 490.
25. Tang C, Livingston MJ, Liu Z, & Dong Z. Autophagy in kidney homeostasis and disease. *Nat Rev Nephrol.* 2020; 16(9):489-508.
26. Ali S & Abdelaziz D. The protective effects of date seeds on nephrotoxicity induced by carbon tetrachloride in rats. *International Journal of Pharmaceutical Sciences Review and Research.* 2014; 26: 62-68.
27. Rahman MM, Muse AY, Khan DMIO, Ahmed IH, Subhan N, Reza HM, Alam MA, Nahar L, Sarker SD. Apocynin prevented inflammation and oxidative stress in carbon tetra chloride induced hepatic dysfunction in rats. *Biomedicine and Pharmacotherapy*; 2017; 92:421-428.
28. Abdelghffar, E. A., Obaid, W. A., Alamoudi, M. O., Mohammedsaleh, Z. M., Annaz, H., Abdelfattah, M. A., & Sobeh, M. Thymus fontanesii attenuates CCl4-induced oxidative stress and inflammation in mild liver fibrosis. *Biomedicine & Pharmacotherapy*, 2022; 148: 112738.
29. Alshammari, G.M., Balakrishnan, A., & Chinnasamy, T. 2-Hydroxy-4-methoxy benzoic acid attenuates the carbon tetra chloride-induced hepatotoxicity and its lipid abnormalities in rats via anti-inflammatory and antioxidant mechanism. *Inflammation Research*, 2017; 66(9): 753-763.
30. Elsayy, H., Badr, G.M., Sedky, A., Abdallah, B.M., Alzahrani, A.M., & Abdel-Moneim, A.M. Rutin ameliorates carbon tetrachloride (CCl4)-induced hepatorenal toxicity and hypogonadism in male rats. *Peer J.*, 2019; 7: 1-20.
31. Alayunt, O., Aksoy, L., Karafakioğlu, Y., & Sevcin Sevimli, S. Assessment of anti-inflammatory and antioxidant properties of safranal on cci4-induced oxidative stress and inflammation in Rats. *An acad brascienc.*, 2019; 91(2): 1-11.
32. Klatt, C., Edward, T., and Vinay, K. Robbins and Cotran Review of Pathology (Robbins Pathology). 5th edition philadelphia, Elsevier 2022; 2(20): 298-317.
33. Chen, L., Deng, H., Cui, H., Fang, J., Zuo, Z., Deng, J., Li, Y., Wang, X., & Zhao, L. Inflammatory responses and inflammation-associated diseases in organs. *Oncotarget*, 9(6): 2017; 7204-7218.
34. Du, J., Zhu, Y., Meng, X., Xie, H., Wang, J., *et al.* Atorvastatin attenuates paraquat poisoning-induced epithelial mesenchymal transition via downregulating hypoxia-inducible factor-1 alpha. *Life Sciences*, 2018; 213, 126-133.
35. Babál P., Kristová V, Cerná A, Janega P, Pechánová O, Danihel L, & Andriantsitohaina R. Red wine polyphenols prevent endothelial damage induced by CCl4 administration. *Physiol Res.* 2006; 55(3):245-251.
36. Kim, H., Jeon, D., Yong Lim, Y., & Jang, I. The effects of coenzyme Q10 supplement on blood lipid indices and hepatic antioxidant defense system in SD rats fed a high cholesterol diet. *Laboratory Animal Research*, 2019; 35: 13.
37. Al-Rekabi, B., Al-Diwan, M., & Sawad, A. The Protective Role of CoQ10 and DHEA and their combination on CCl4 induced liver injury in adult male rats (*Rattus norvegicus*). *Journal of Bioscience and Applied Research*, 2019; 5(3), 375-389.
38. Yubero, D., Montero, R., Martín, M., Montoya, J., Ribes, A., Grazina, M., Trevisson, E., Rodriguez-Aguilera, J., Hargreaves, I., & Salvati, L. CoQ deficiency study group. Secondary coenzyme Q10 deficiencies in oxidative phosphorylation (OXPHOS) and non-OXPHOS disorders. *Mitochondrion*, 2016; 30, 51-58.
39. Youssef, G., Al Anany, M., Salah El-din, G., & Mousa, S. The effect of coenzyme Q10 and/or silymarin on renalase gene expression of cardiorenal syndrome in adult male albino rats. *Al-Azhar Med. J.*, 2018; 47(3): 645-658.
40. Zhai, J., Bo, Y., Lu, Y., Liu, C., & Zhang, L. Effects of Coenzyme Q10 on Markers of Inflammation: A Systematic Review and Meta-Analysis. *PloS one*, 2017; 12(1): e0170172.
41. Chen, P.P., Xu, H.L., Ting-Yue, ZhuGe, D.L., Jin, B.H., Zhu, Q.Y., Shen, B.X., Wang, L.F., Lu, C.T., Zhao, Y.Z., & Li, X.K. CoQ10-loaded liposomes combined with UTMD prevented early nephropathy of diabetic rats. *Oncotarget.*, 2018; 9(14): 11767-11782.
42. Othman, A.A., Shoheib, Z.S., Abdel-Aleem, G.A., & Shareef, M.M. Experimental schistosomal hepatitis: protective effect of coenzyme-Q10 against the state of oxidative stress. *Experimental parasitology*, 2008; 120(2): 147-155.
43. Kim, J., & Park, E. Coenzyme Q10 attenuated DMH-induced precancerous lesions in SD rats. *J Nutr Sci Vitamino.*, 2010; 56(2): 139- 144.
44. Zhang, D., Yan, B., Yu, S., Zhang, C., Wang, B., Wang, Y., Wang, J., Yuan, Z., Zhang, L., & Pan, J. Coenzyme Q10 inhibits the aging of mesenchymal stem cells induced by D-galactose through Akt/mTOR signaling. *Oxidative medicine and cellular longevity*, 2015: 867293. <https://doi.org/10.1155/2015/867293>.
45. Zhang, X., Shi, Z., Liu, Q., Quan, H., & Cheng, X. Effects of coenzyme Q10 intervention on diabetic kidney disease. *Medicine*, 2019; 98 (24): 1-18.

46. El-Sokkary, Gamal & Awadalla, Eatemad: The Protective Effect of Saffron (*Crocus sativus* L.) against Carbon Tetrachloride Induced Toxicity in Some Organs of Albino Rats. *Egyptian Academic Journal of Biological Sciences, B. Zoology*. (2019). 11. 1-18. [10.21608/eajbsz.2019.31092](https://doi.org/10.21608/eajbsz.2019.31092).

## الملخص العربي

## دراسة نسيجية وكيميائية مناعية عن الدور الوقائي لمساعد الإنزيم Q10 في السمية المستحثة من رابع كلوريد الكربون على القشرة الكلوية للذكور البالغين من الجرذان البيضاء

أسماء إبراهيم أحمد وهاجر يسري راضي

قسم التشريخ وعلم الأجنة، كلية الطب، جامعة عين شمس، القاهرة، مصر

**المقدمة:** رابع كلوريد الكربون هو سم كيميائي يسبب الإجهاد التأكسدي. مساعد الإنزيم Q10 هو أحد مضادات الأكسدة الطبيعية الموجودة في اللحم والأسماك والمكسرات وبعض الزيوت.

**الهدف من العمل:** تقييم التأثير الوقائي لمساعد الإنزيم Q10 على إصابة الكلى بعد التعرض لرابع كلوريد الكربون **المواد والطرق:** أربعة وأربعون ذكور الجرذان البيضاء البالغة مقسمة إلى ثلاث مجموعات. المجموعة الأولى (المجموعة الضابطة) تضمنت 24 فأراً، المجموعة الثانية (المجموعة المعالجة برابع كلوريد الكربون) تضمنت 10 فئران تم حقنها داخل الصفاق بمحلول رابع كلوريد الكربون بجرعة 0.1 مل / 100 جم من وزن الجسم. مرتين أسبوعياً لمدة أسبوعين. المجموعة الثالثة (المجموعة المعالجة بمساعد الإنزيم Q10 + رابع كلوريد الكربون): تضمنت 10 فئران تلقت حقنات مصاحبة داخل الصفاق من CCl4 بنفس الجرعات وبنفس المدة كما في المجموعة الثانية، بالإضافة إلى CoQ10 بجرعة 10 مجم / كجم من وزن الجسم / يوم.

في نهاية التجربة، تم التضحية بجميع الفئران؛ تم تشريح الكلى ومعالجتها للفحص المجهرى الضوئي والالكتروني تم إجراء الفحص المناعي لـ iNos. تم تحليل النتائج إحصائياً.

**النتائج:** يتسبب رابع كلوريد الكربون في حدوث تشوه ملحوظ في بنية القشرة الكلوية. أظهر فحص المجهر الضوئي زيادة خلوية في الحزمة المركزية من الشعيرات الدموية في الخصلة الكبيبية مع صغر مساحة محفظة بومان. حدث التصاق الخصلة الكبيبية بالطبقة الجدارية لكبسولة بومان. كما تم الكشف عن انكماش للزوائد الاصبعية للخلية بودوسيت بواسطة المجهر الالكتروني.

كشفت الأنابيب القشرية الكلوية عن تغيرات تنكسية ونخرية. أظهر النسيج الخلالي تسلل الخلايا الالتهابية وحيدة النواة وبالتالي التليف. تم تأكيد ذلك من خلال زيادة منوية ذات دلالة احصائية عالية في مساحة ألياف الكولاجين. أظهر الفحص المناعي لـ iNos زيادة منوية في المجموعة المعالجة برابع كلوريد الكربون مقارنة بالمجموعة الضابطة والمجموعات المعالجة. أظهر تحليل وظائف الكلى BUN والكرياتينين زيادة منوية ذات دلالة احصائية عالية في المجموعة الثانية مقارنة بالمجموعة الأولى والثالثة. تم تحسين كل هذه التغييرات عن طريق إعطاء مساعد الإنزيم Q10 للمجموعة الثالثة.

**الاستنتاجات:** مساعد الإنزيم Q10 يمكن أن يحمي من إصابة الكلى التي يسببها رابع كلوريد الكربون.